Fabrication of metallic nanowires and nanoribbons using laser interference lithography and shadow lithography

2010 Nanotechnology 21 215301

(http://iopscience.iop.org/0957-4484/21/21/215301)

Nanotechnology **21** (2010) 215301 (6pp) doi:10.1088/0957-4484/21/21/215301

Fabrication of metallic nanowires and nanoribbons using laser interference lithography and shadow lithography

Joong-Mok Park[1], Kanwar Singh Nalwa[2], Wai Leung[1], Kristen Constant[3], Sumit Chaudhary[2,3] and Kai-Ming Ho[1]

[1] Ames Laboratory-USDOE and Department of Physics and Astronomy, Iowa State University, Ames, IA 50011, USA
[2] Department of Electrical and Computer Engineering, Iowa State University, Ames, IA 50011, USA
[3] Ames Laboratory-USDOE and Department of Materials Science and Engineering, Iowa State University, Ames, IA 50011, USA

E-mail: joongmok@iastate.edu

Received 8 January 2010, in final form 7 April 2010
Published 30 April 2010
Online at stacks.iop.org/Nano/21/215301

Abstract
Ordered and free-standing metallic nanowires were fabricated by e-beam deposition on patterned polymer templates made by interference lithography. The dimensions of the nanowires can be controlled through adjustment of deposition conditions and polymer templates. Grain size, polarized optical transmission and electrical resistivity were measured with ordered and free-standing nanowires.

(Some figures in this article are in colour only in the electronic version)

1. Introduction

Recently, nanostructured materials have been actively studied due to their novel electronic, optical and mechanical properties [1–3]. Such semiconducting, oxide or metallic structures can show quite different properties from those of bulk materials. One-dimensional metallic nanostructures such as nanorods, nanowires and nanoribbons are of special interest due to their simple nanoscale nature and recent developments in fabrication methods. When combined with active functional devices such as photovoltaic or light-emitting devices, their unique properties can enhance device performance. Metallic nanowires have potential applications in electronic [4–6], optoelectronic [7] and mechanical devices [8] as well as importance in fundamental studies of nanostructured material itself.

A variety of techniques have been investigated and developed to make metallic nanowires and nanoribbons. Top-down methods that involve transferring patterned templates to fabricate nanowires include conventional lithography [9] and nanoimprinting [10]. Bottom-up approaches include self-assembly and electrochemical deposition within templates [6, 11]. Each has advantages and disadvantages either in processing efficiency or quality and reproducibility of the resulting structures.

Here we describe a simple, cost-efficient and mass-producible method of fabrication for producing metal nanowires and nanoribbons in a two-step process. First, a contact mask is fabricated with a photosensitive material, photoresist, using two-beam laser holography [12]. The second step is metal coating by physical vapor deposition using shadow edge lithography [13, 14] either in single-or multi-stage depositions. Nanowires are defined in this paper as straight as-deposited, whereas nanoribbons are broken and curved as compared to their configuration during growth. The dimensions of the nanowires can be controlled by the photoresist patterns and deposition conditions such as angle and thickness. Few-centimeter-long nanowires and nanoribbons were made with this method. Also e-beam physical vapor deposition can deposit large numbers of materials in making nanowires. Their structural, optical and electrical properties are characterized by scanning electron microscopy (SEM), transmission electron microscopy (TEM), atomic force microscopy (AFM) and four-probe resistivity

measurements. These fabrication methods can be used for most metals (and even semiconductors or insulators even though they have poor electrical conductivity) to form nanowires and nanoribbons.

2. Experimental details

To fabricate nanowires and nanoribbons, first, photoresist was patterned on a substrate with laser interference. The patterns developed after exposure are used as deposition masks. Nanowires and nanoribbons of submicron width and a few centimeters long have been fabricated using normal and shadow deposition. Physical vapor deposition using e-beam evaporation is used to deposit a variety of metals on the photoresist mask.

2.1. Polymer template fabrication

We used a Lloyd's mirror set-up for photoresist patterning. An Ar-ion laser with a wavelength of 364 nm is used as the coherent light source. A spatial filter, 10× ultraviolet objective lens and 10 μm diameter pinhole, expands the beam and makes it homogeneous. The distance between the spatial filter and sample is 2 m, which is far enough to ignore beam divergence and results in a large exposed area. In this configuration, the pitch can be adjusted by changing the incidence angle by simultaneously rotating the stage with sample and mirror. A photoresist (HiR 1075 from AZ Electronics) is spin-coated on the substrate, exposed and then developed for 60 s in MIF 300 developer.

2.2. Metal deposition

Physical vapor deposition using e-beam evaporation is used to deposit a variety of metals on the photoresist mask. The distance between the sample and evaporation source is about 1 m, so the deposition is approximately collimated. A quartz crystal monitor was used to monitor the deposition rate and thickness during the deposition. The deposition rate was maintained at about 1 Å s^{-1}. The pressure was below 10^{-6} Torr during the deposition. Deposition normal to the plane of the photoresist patterned substrate results in thin metal films both on top of the photoresist lines and between lines in the channels as figure 1(a). Deposition with tilted angles can deposit metals on one of the sidewalls of the photoresist and some bottom area of the channel as well as on the top surface of the photoresist as in figure 1(c). The deposition width on the bottom of the channel depends on the periodicity, thickness and width of the photoresist and the angle of deposition. We can choose the pitch, width and thickness of the deposited materials by simply rotating the Lloyd's mirror, and altering the metal deposition rate and time.

2.3. Four-point resistivity measurement

In order to measure the electrical resistance of nanoribbons, four-point probes (FPP) were made of Al on oxidized silicon wafers and transferring the nanoribbons on these patterns. The distances between two inner probes was set at 50 μm. Transferring the nanoribbons on these patterns could not be accomplished by drop-casting from a dispersion in isopropyl alcohol because the nanoribbons have a tendency to agglomerate near the metal probes and did not establish an electrical path between the probes. A nanoribbon network between the probes was created by filtering the nanoribbons dispersed in isopropyl alcohol through a cellulose filter of 0.22 μm pore size (Millipore). A continuous network of nanoribbons was obtained by vacuum filtration through the cellulose filter. The filter was stamped with the probe pattern under a pressure of 6.9 kPa over 12 h. The filter was dissolved using acetone and the pattern was used to perform four-point resistivity measurements. In order to find the temperature dependence of resistivity, the wafer was heated to 366 K and resistance was measured while cooling.

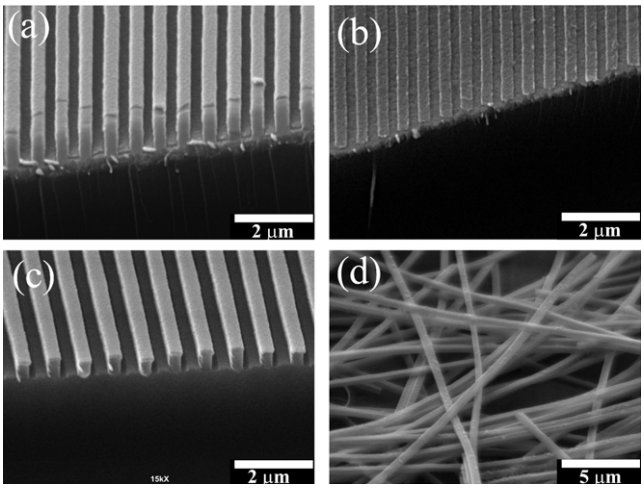

Figure 1. (a) SEM image of 50 nm Al deposited at normal incidence on 250 nm wide photoresist bars with 550 nm period. (b) Al wires of width 250 nm and 50 nm thick on indium tin oxide glass substrate after removal of photoresist. (c) 100 nm Ti deposited with 15° tilted angle from normal direction. (d) Ti nanoribbons after removal from substrate.

3. Results and discussion

After deposition, the photoresist is removed by immersing in photoresist stripper, Remover PG (MicroChem Corp.), for 30 min and the samples were dried with N_2 gas after rinsing with IPA (isopropyl alcohol) twice. The metal nanowires deposited in the channels of the pattern remain even after chemical removal of the photoresist, as in figure 1(b), whereas thin metallic films deposited on top of the pattern are detached during the rinsing process. These materials can be recovered as nanoribbons which have the same thickness and roughly the same width of patterns on the substrate. Curled nanoribbons as in figure 1(d) are collected by dispensing a few drops of IPA containing nanoribbons on a flat substrate and vacuum-assisted drying. To determine the dimensions and surface roughness AFM imaging was performed on Au and Al nanowires on an Si substrate. Cross-sectional AFM images show the rectangular shapes of 500 nm wide and 100 nm thick Al wires and 500 nm wide and 80 nm thick Au wires as in figures 2(a) and (c). The

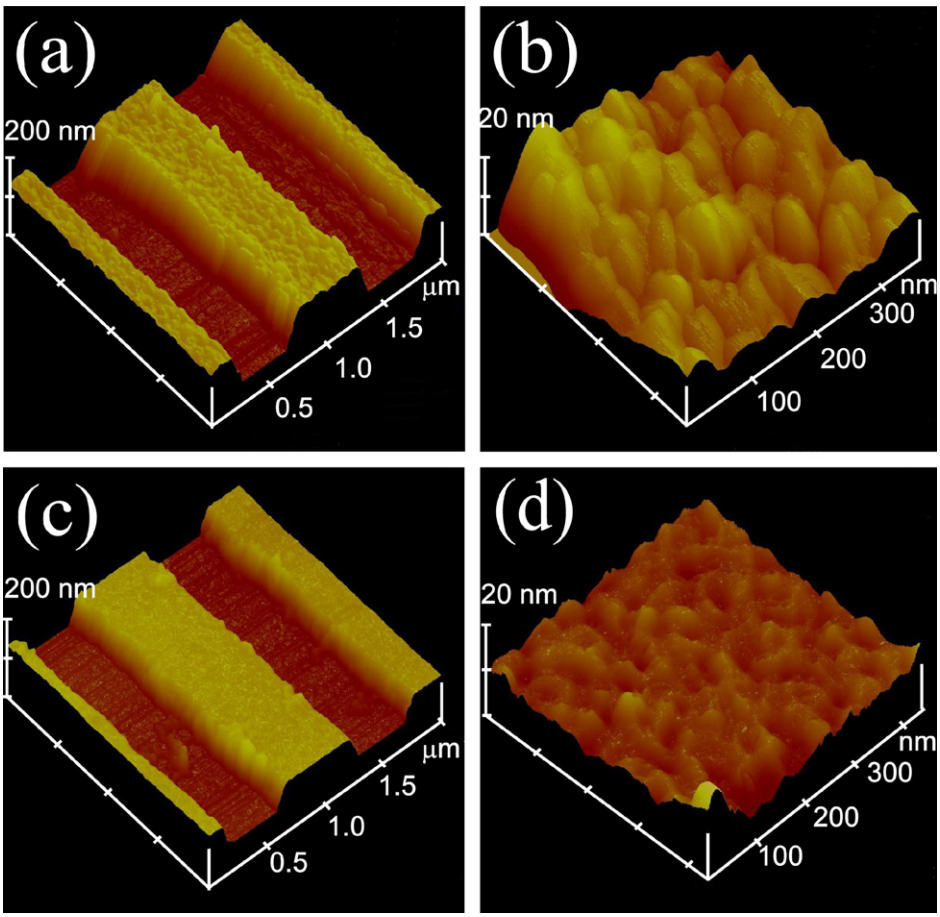

Figure 2. (a) AFM image of Al wires of 500 nm wide and 100 nm thick on the Si substrate after removal of photoresist and (b) surface image. (c) Au wires of 500 nm width and 80 nm thick on the Si substrate and (d) surface image.

average surface roughness of the metal wires is about 2.5 nm for Al wires and 1.0 nm for Au wires as in figures 2(b) and (d).

Multiple depositions from different directions can result in a more narrow (scalable to sub-100 nm width) metal deposition on the substrate as shown in figure 3. The normal deposition path is narrowed by metal previously deposited in angled depositions. After removal of the remaining photoresist, Al wires have a narrower width of 150 nm compared to the width of 300 nm by single normal deposition. The top part of the Al wires detach when dissolving the photoresist and a second layer of Al wires can be deposited, forming a two-layer crossed-mesh structure. The center line of Al of the second layer is not as straight as the first layer because of diffraction of the first Al layer during photoresist patterning. The reflected beam from diffracted light from the first Al structure disrupts the second layer structure during subsequent photoresist patterning. Also the spin coating of the second photoresist layer on the rough surface is not as uniform as those coated on a flat substrate. This structure shows high optical transmission in the visible and near-IR wavelengths and can be used as a transparent electrode for organic/inorganic light-emitting devices and solar cells.

We measured normal, specular transmission of Al nanowires as in figure 3(b) with a fiber coupled spectrometer (Ocean Optics) in the visible to near-IR spectral range (400–1000 nm). Al nanowires have a period of 700 nm (thickness of 150 nm and width of 100 nm) and are made on a 200 μm thick glass substrate for transmission measurements. A Glan–Taylor polarizer was used to polarize the light. Wavelengths greater than the grating period of 700 nm have higher transmission for both polarizations. The difference between the two polarizations is most clearly seen around 530 nm. This is the second-order diffraction of the glass–nanowire interface. Multiplying the period by the refractive index of glass, 1.52, and dividing by 2 yields 532 nm. Typically p-polarized light (perpendicular to the grating) has more transmission than s-polarized light for wire grid polarizers but this result is opposite to expectations. This is explained by the fact that the grating period is large compared to those of metal grid polarizers working in the visible spectrum range [4]. Also, the narrow metallic wire structures have a greater open area so it has high transmittance. Even though the Al nanowires show little polarization dependence in the visible spectral range, high transmission is useful for transparent electrodes.

To examine the grain structure of nanoribbons, TEM images were taken. Nanoribbons suspended in isopropyl alcohol were ultrasonicated for 1 min to break them into small pieces. The broken nanoribbons were deposited on carbon grids by dropping with isopropyl alcohol and vacuum-assisted drying. The average grain size of Al nanoribbons is about

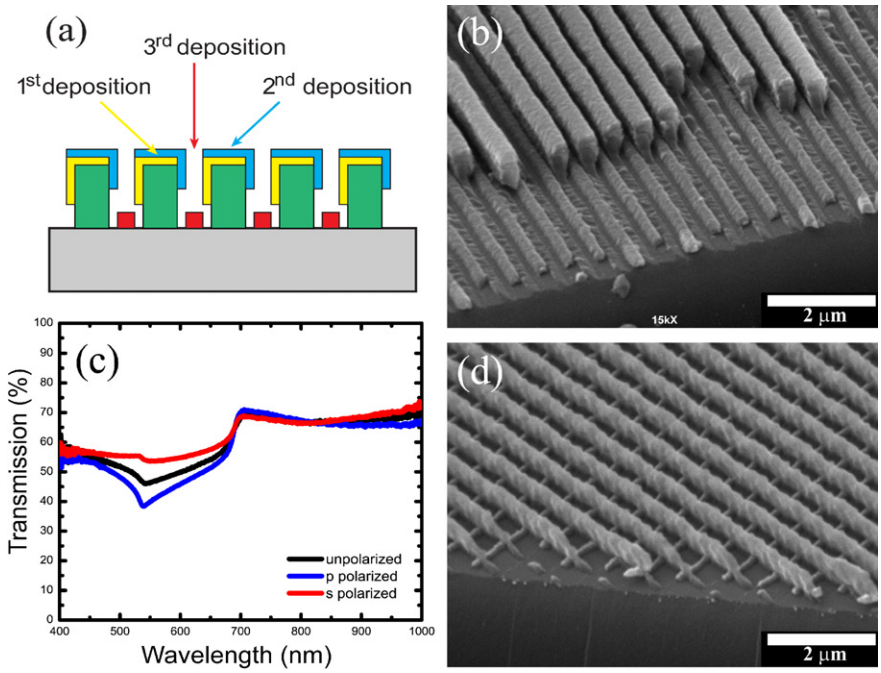

Figure 3. (a) Schematic diagram for three angle depositions at +45°, −45° and 0°. (b) After three depositions, center wires have bar width—-approximately 150 and 100 nm thickness. (c) Transmission spectra of Al nanowires on glass substrate. The period of Al is 700 nm and height and width are 150 and 100 nm. Electric field of the p-polarization is perpendicular to the grating. (d) Two layers of Al nanowires cross-patterned on top of center lines.

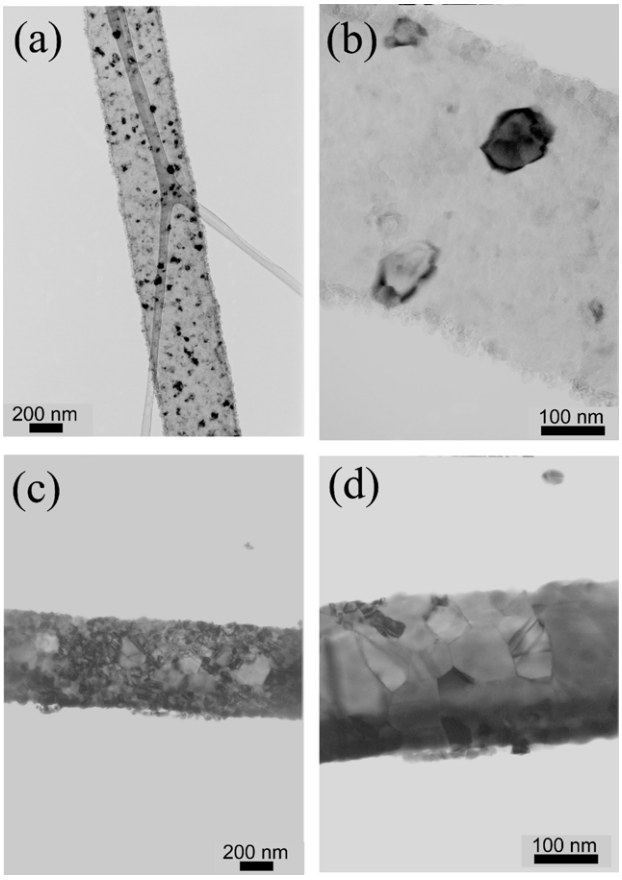

Figure 4. (a) Bright-field TEM image of Al ribbon of 500 nm wide and 100 nm thick (b) and *in situ* annealed at 600 °C. (c) Au ribbon of 300 nm wide and 80 nm thick as deposition (d) and *in situ* annealed at 650 °C.

10–20 nm by TEM as shown in figure 4(a). Au appears to have a larger grain size than Al, about 50 nm. Also, although it is thinner, an Au ribbon has a darker image than an Al ribbon due to its larger atomic number. The grain size depends on various deposition conditions (materials, impurities, temperature, substrate, etc). Thermal annealing can increase the grain size and enhance electrical conductivity for nanoribbons but there are some limitations to grain growth related to the small dimensions of nanoribbons. We observed the grain growth during an *in situ* annealing process. For the Al case, there was no substantial grain growth and after annealing at 600 °C for 2 h (melting temperature of Al is 660 °C). Grain growth was more substantial in Au nanoribbons annealed at 650 °C, which is well below its melting temperature (1063 °C), because there is little oxide and the initial grains are much larger.

Figure 5(a) shows the network of Al nanoribbons (300 nm width and 150 nm thickness), on a cellulose filter obtained by vacuum filtration. The figure illustrates that the network is dense enough to be suitable for making transparent electrodes from nanoribbons for organic light-emitting devices (OLEDs) and photovoltaic applications. Currently, the transfer process (from the cellulose filter to the FPP pattern) has not been optimized, and only a fraction of the nanoribbons are transferred. The process will be further optimized to ensure uniform nanoribbon distribution on an mm–cm scale. However the current distribution of Al nanoribbons on FPP is sufficient for measuring the resistance of individual nanoribbons. There was a mesh of nanoribbons between the outer electrodes as in figure 5(b), leading to several conducting pathways between outer and inner electrodes. However, the inner electrodes were only bridged by single nanoribbons. The number of such single

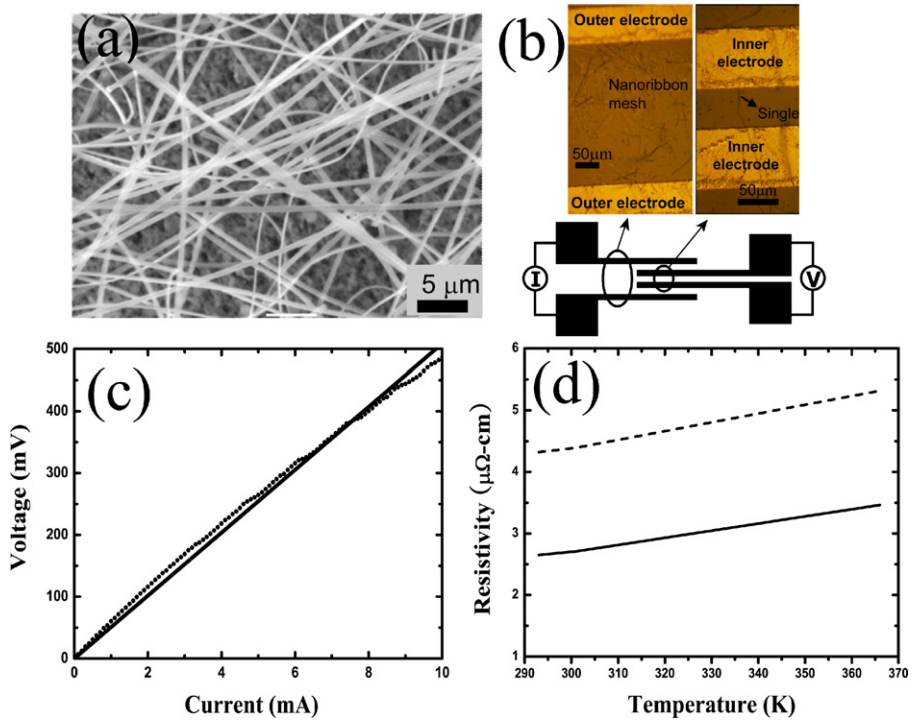

Figure 5. (a) SEM image of Al nanoribbon network on cellulose filter and (b) optical microscope images of four-point probe electrodes with nanoribbons. (c) I–V curve obtained using four-point resistivity measurement of single nanoribbon (dotted) with fitted line. (d) Temperature dependence resistivity of single Al nanoribbon (dashed) and Al bulk (line) from 293 to 366 K by four-point resistivity measurements.

nanoribbons was counted and resistivity of a single nanoribbon was estimated.

The I–V curve as shown in figure 5(c) exhibits ohmic electrical behavior of the Al nanoribbon, with resistance ∼50 Ω. The resistivity of an individual nanoribbon, ρ was calculated from: $\rho = AR/L$, where A is the cross-sectional area of the nanoribbon and L is the electrically isolated length. Taking the width ∼300 nm, thickness ∼150 nm and length ∼50 μm, the resistivity is 4.32 ± 0.12 $\mu\Omega$ cm, which is higher than the bulk resistivity value (∼2.65 $\mu\Omega$ cm) [15]. It is well known that the resistivity increases when the electron mean free path is larger than the dimension of nanowires [16]. Surface scattering and grain boundary scattering of electrons explain the resistivity increase in nanowires. Additionally, Al has a thin (∼10 nm) native oxide layer on the surface. For bulk or thick films, the oxide layer does not affect resistivity but when the dimension of nanoribbons is close to the thickness of the oxide layer, the increase in resistivity is expected. Figure 5(d) shows the temperature dependence of the resistance of single nanoribbons [17, 18]. The resistance is found to increase with temperature for both Al bulk and nanoribbons: however, the slope ($\mathrm{d}R/\mathrm{d}T$) is slightly different for the two cases [19, 20]. The temperature dependence of resistivity can be explained by electron–phonon scattering.

4. Conclusions

In summary, we fabricated metallic nanowires and nanoribbons with the combination of laser interference holography and e-beam metal deposition. This fabrication method can produce well-defined, rectangular cross-sectioned nanowires with dimensions of a few cm long and submicron width, both on a substrate and as a free suspension. Nanowires on a substrate can be further processed to make the desired cross-mesh structures, and detached nanoribbons can be processed or stamped as random meshes on another substrate. Structural properties of metallic nanowires and nanoribbons were characterized using SEM, AFM and TEM. Electrical resistivity of Al nanoribbons was also measured. Potential applications of one-dimensional nanostructures in this report include electrodes for cross-bar electronic devices like memories, and conducting as well as transparent electrodes for light-emitting-diodes and photovoltaic cells.

Acknowledgments

This work is supported by the Director for Energy Research, Office of Basic Energy Sciences. The Ames Laboratory is operated for the US Department of Energy by Iowa State University under contract no. DE-AC02-07CH11358.

References

[1] Pauzauskie P J and Yang P 2006 *Mater. Today* **9** 36–45
[2] Chen Y and Goldman A M 2008 *J. Appl. Phys.* **103** 054312
[3] Wu Y, Xiang J, Yang C, Lu W and Lieber C M 2004 *Nature* **430** 61–5
[4] Chen L, Wang J J, Walters F, Deng X, Buonanno M, Tai S and Liu X 2007 *Appl. Phys. Lett.* **90** 063111

[5] Xiang C, Kung S-C, Taggart D K, Yang F, Thompson M A, Guell A G, Yang Y and Penner R M 2008 *ACS Nano* **2** 1939–49
[6] Peng Y, Cullis T and Inkson B 2008 *Appl. Phys. Lett.* **93** 183112
[7] Kang M-G and Jay Guo L 2007 *Adv. Mater.* **19** 1391–6
[8] Wu B, Heidelberg A and Boland J J 2005 *Nat. Mater.* **4** 525
[9] Guo H C, Nau D, Radke A, Zhang X P, Stodolka J, Yang X L, Tikhodeev S G, Gippius N A and Giessen H 2005 *Appl. Phys.* B **81** 271–5
[10] Jay Guo L 2007 *Adv. Mater.* **19** 495–513
[11] Shantha Shankar K and Raychaudhuri A K 2005 *Mater. Sci. Eng.* C **25** 738–51
[12] Onoa G B, O'Reilly T B, Walsh M E and Smith H I 2005 *Nanotechnology* **16** 2799–803
[13] Bai J G, Chang C-L, Chung J-H and Lee K-H 2007 *Nanotechnology* **18** 405307
[14] Xue M, Yang Y and Cao T 2008 *Adv. Mater.* **20** 596–600
[15] Lide D R 1997 *Handbook of Chemistry and Physics* (Boca Raton, FL: CRC Press)
[16] Sun T, Yao B, Warren A P, Barmak K, Toney M F, Peale R E and Coffey K R 2009 *Phys. Rev.* B **79** 041402
[17] Tian M, Wang J, Zhang Q, Kumar N, Mallouk T E and Chan M H W 2009 *Nano Lett.* **9** 3196
[18] Wang J, Shi C, Tian M, Zhang Q, Kumar N, Jain J K, Mallouk T E and Chan M H W 2009 *Phys. Rev. Lett.* **102** 247003
[19] Mani S, Saif T and Han J H 2006 *IEEE Trans. Nanotechnol.* **5** 138
[20] Bid A, Bora A and Raychaudhuri A K 2006 *Phys. Rev.* B **74** 035426